Applied Acoustics 214 (2023) 109710

Contents lists available at ScienceDirect

Applied Acoustics

journal homepage: www.elsevier.com/locate/apacoust

Influence of noise masking on leak pinpointing: Experimental analysis on a laboratory test rig for leak noise correlation.

Andrea Santoni *, Irene Marzola, Stefano Alvisi, Patrizio Fausti, Cesare Stefanelli

Department of Engineering, University of Ferrara, via G. Saragat 1, 44122 Ferrara, Italy

ARTICLE INFO

Keywords:
Water leak
Acoustic correlation
Vibroacoustic analysis
Signal filtering
Noise masking

ABSTRACT

The efficient management of water distribution networks requires the detection and mitigation of leaks that result in significant water losses, economic costs, and potential health hazards. This experimental study focuses on the optimal frequency range for accurately locating a water leak in a distribution network using the noise correlation approach while mitigating the influence of background noise associated with water consumption from users. Through laboratory experimental tests, a digital bandpass filter was defined in order to pre-process signals and to improve cross-correlation analysis within the pertinent frequency range. This was done by characterising the frequency content of leak-induced noise, noise masking resulting from water consumption, and background noise. The analysed signals were recorded using hydrophones installed within the pipes of a laboratory test rig under different conditions of water flow rate. The spectra analysis assessed the influence of varying water flow rates on the acoustic sound field within the pipeline system. Additionally, the results of the analysis made it possible to discriminate clearly between noise generated by leaks and noise attributed to water consumption. This distinction is useful for implementing suitable filters, and also to establish a threshold ratio of leak flow rate to water consumption flow rate for effective pre-filtering. This study aims to establish a methodological framework that can effectively differentiate between acoustic signals stemming from leaks and noise generated by other sources within the system, to improve leak location accuracy through the noise correlation approach.

1. Introduction

Water utilities and water management authorities continuously endeavour to enhance the efficiency of water distribution networks. Leakages, occurring at various points in the network such as joints, valves, and pipes, lead to water losses ranging from less than 5% to over 50% [1,2]. Besides wasting a valuable natural resource, leakages cause significant economic costs and pose health risks due to potential contamination of drinkable water [3]. To address these challenges, water utilities employ diverse approaches to promptly detect and minimise the impact of leaks [4,5], encompassing thermography, ground penetrating and subsurface radars, tracer gas, earth sensitivity changes, and acoustic methods for both leak detection and pinpointing [6,7]. Acoustic methods, which are comprehensively reviewed in the subsequent section, hinge upon the utilization of the cross-correlation technique. This technique is employed to estimate the location of a leak within a given system. It relies on the cross-correlation function derived from two distinct signals acquired via accelerometers or hydrophones. To ensure accurate and reliable results, the influence of sound sources unrelated with the leak's presence must be mitigated.

The central objective of this investigation is to systematically characterise the influence of varying water flow rates on the acoustic sound field within the pipeline system. Additionally, this study aims to establish a methodological framework that can effectively differentiate between acoustic signals stemming from leaks and the noise generated by other sources within the system. Specifically, this research focuses on the identification of a distinct frequency range that characterises the noise produced by leaks within a specific segment of the network, in which the influence of background noise arising from water consumption can be minimised. Unlike other masking sound sources like traffic noise, which can be monitored and mitigated by recording signals during quieter periods, monitoring water consumption is more challenging. The frequency content in the water distribution system is analysed in different operating conditions in order to characterise: the system's background noise in the stationary standard condition (with no water flow), leak-generated noise, and masking noise generated by water consumption. Spectral analysis is used to design of a digital bandpass

* Corresponding author.
E-mail address: andrea.santoni@unife.it (A. Santoni).

https://doi.org/10.1016/j.apacoust.2023.109710
Received 10 January 2023; Received in revised form 18 October 2023; Accepted 19 October 2023
Available online 28 October 2023

filter to pre-process the signals. This filter restricts the cross-correlation analysis to the frequency range affected by the leak-generated noise, minimising the influence of noise associated with water consumption. The results of such analysis help identify a maximum threshold of the ratio of leak flow rate to water consumption flow rate up to which pre-filtering effectively reduces the noise masking effect, increasing the accuracy of the cross-correlation approach in locating the leak within the system.

It is important to emphasize that this study does not introduce new signal processing methodologies. Instead, its primary focus is on presenting a systematic approach to characterise the acoustic field originating from diverse sound sources within a designated segment of the water distribution network. Such an approach holds potential for pre-filtering the signals employed in the correlation-based technique used to pinpoint leaks. The novelty of this study resides in its comprehensive analysis of the frequency content present within the piping system across varying acoustic conditions. This analysis enables a clear discrimination between noise generated by leaks and noise attributed to water consumption, ultimately facilitating the implementation of suitable filters. Through this research, we aim to contribute to advancements in leak detection methods, optimising water distribution networks and minimising water losses. The proposed approach could be iteratively implemented by water utility companies in in-situ conditions with the widespread use of low-cost vibroacoustic sensors in water distribution networks, enhancing leak detection accuracy and assisting in water resource conservation and public health and safety.

The following section reviews the state of the art in leak detection based on noise correlation through an extensive literature review. Section 3 describes the experimental laboratory test rig and the methodology employed to evaluate leak positions through noise correlation. Section 4 presents the results of this experimental study, followed by a discussion on the influence of water consumption from users on the sound field within a water distribution network and, ultimately, an assessment of its effect on the accuracy and reliability of the cross-correlation technique.

2. State of the art on acoustic leak location

The leak detection activity can be generally broken down into two main phases (although a three-phase categorization was also proposed [8]). The *location phase* refers to the identification of potential leakages within a specific area of the water distribution system or along a particular branch, while *pinpointing techniques* are employed to precisely evaluate the leak position, varying depending on the system's characteristics. Acoustic techniques can be used to identify the presence of a leak in a specific branch of the distribution system (listening devices), and they can also be effective in leak pinpointing (leak noise correlators).

In the late '80s, the Fraunhofer Institut for Building Physics (Fraunhofer-Institut für Bauphysik - IBP) developed and tested an efficient system for leak pinpointing known as LOKAL, using a dual-channel acquisition system enabling FFT (Fast Fourier Transform) analysis [9]. Over the years, acoustic leak pinpointing approaches have proven to be reliable tools, providing good accuracy for distances up to 500 m in metal pipes [10]. However, in plastic pipes - polyvinyl chloride (PVC) or polyethylene (PE) - acoustic leak location is far more challenging and applicable only over shorter distances ($<<$ 100 m) due to the higher attenuation rate presented by the system [11]. The acoustic leak pinpointing technique relies on the cross-correlation of two vibroacoustic signals recorded on access points of the network, placed on both sides of the suspected leak location. The reliability of this experimental approach depends on two factors: first, a reliable estimate of the time delay between the two signals, obtained by maximising the cross-correlation function (CCF). Secondly, on an accurate prediction of wave propagation velocity, influenced by the pipe's characteristics, the fluid within, and the soil burying the pipe [12]. Fundamental research focusing on the physics governing the fluid-structure-soil mutual interaction, combined with experimental testing, has continuously improved the reliability of this method, leading to a comprehensive understanding of how the vibroacoustic perturbance propagates along the fluid-filled pipe [13]. Several analytical models have been proposed to compute the sound wave propagation velocity from the properties of the fluid and the geometrical and elastic characteristics of the pipe. Some models consider a pressure wave propagating through an inviscid compressible fluid contained in a cylindrical elastic shell [14–19]. Other models, more suitable for buried pipes, additionally consider the effect of the soil on wave propagation [20–22]. As shown by Muggleton et al. [23], the approximated analytical formulations allow for an accurate estimate of the propagation velocity, even in plastic pipes, up to 1/4 of the system's ring-frequency. Accurately estimating the time delay between the two signals requires a good signal-to-noise ratio (SNR) to maximise the peak in the CCF. For this purpose, the choice of sensors is crucial, especially in systems characterised by a high attenuation rate [24]. Accelerometers generally provide a more pronounced peak in the CCF, although hydrophones, guaranteeing a higher signal-to-noise ratio (SNR), are more suitable in plastic pipes [25,26]. Extensive field testing on plastic buried pipes was performed by Hunaidi et al. [3,12] to characterise leak signals and assess the reliability of the noise correlation approach. The investigation considered various aspects, such as sensor positioning, pipe pressure, and flow rate, leading to results exhibiting an accuracy of within 5 m in locating the leak position, which could be increased to 1 m by correcting the propagation velocity provided by commercial correlators. Brennan et al. [27,28] compared different correlators through a virtual test rig, where the vibrational field on the pipe surface was excited by a small loudspeaker. Their findings showed good reliability only in a limited range of frequencies, probably due to the characteristics of the employed sound source. Despite recording signals during the quietest periods and those with minimum water consumption, background noise potentially masks the leak noise, reducing the accuracy of the cross-correlation time delay estimate. To obtain a sharper peak in the CCF and increase accuracy in locating leaks, Gao et al. [29] analysed the use of the general cross-correlation (GCC) algorithm instead of the basic cross-correlation (BCC) algorithm. They found that pre-filtering the signals using the GCC algorithm improved the accuracy in locating the leak. More advanced techniques, such as time-frequency analysis through the wavelet transform (WT) or the short time Fourier transform (STFT) [30–33], have been proposed to reduce background noise influence and improve the accuracy of acoustic approaches for leak detection and location.

Statistical and machine learning techniques can be used to improve the efficiency and reliability of traditional leak detection methods [34]. The application of these approaches has been investigated to identify leaks in water systems and gas distribution pipelines [35,36]. A few commercial solutions that use machine learning for leak location and pinpointing are also available. For example, the company FIDO Tech uses multiple smart devices, with vibro-acoustic sensor and data logger, combined with differential analysis and machine learning to detect and locate leaks [37]. Their algorithms can filter out non-leak noises such as pumps, sudden high customer water usage, or traffic, and they can also estimate the size of a leak. In the future, it is expected that there will be an increase in the use of continuous monitoring of distribution networks, which can improve the efficiency of leak detection, through IoT transducer arrays [38], using low-cost miniature sensors known as MEMS (Micro Electro-Mechanical Systems). To the best of the authors' knowledge, a commercial solution of MEMS hydrophones, which would present many advantages over accelerometers especially in plastic pipe networks, is not yet available, but laboratory prototypes have been successfully developed [39,40].

As shown by a recent study published by Yu et al. [41], despite recent advances, leak detection in water distribution networks is still typically performed manually by field operators. This process is time-consuming, resource-intensive, and can be subjective, depending on the

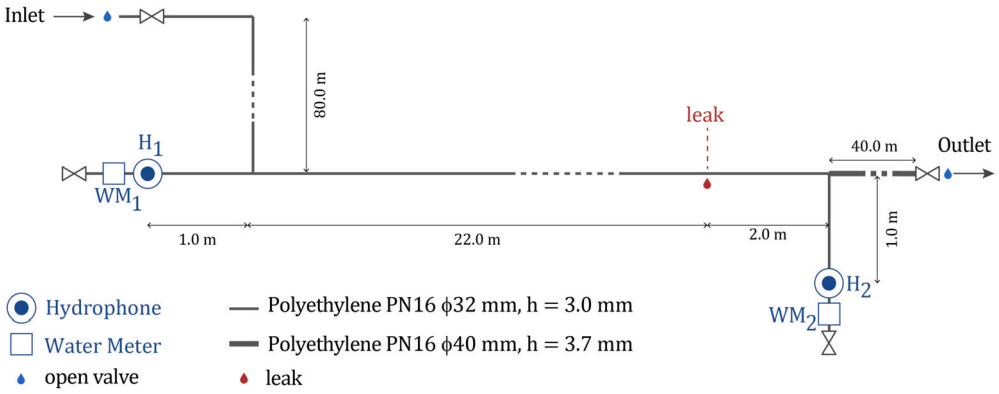

Fig. 1. Diagram of the experimental test rig.

operator's level of expertise. This paper proposes a methodology to discriminate between leak signals and system background noise to address this issue, which could be employed for supervised training and calibration steps of an automated signal analysis system of vibroacoustic signals recorded by a distributed array of sensors.

3. Materials and methods

3.1. Experimental measurements

Sound pressure measurements and audio recordings were carried out on an experimental test rig set up at the Engineering Department laboratories of the University of Ferrara. The test rig consisted of an unburied pipe system, approximately 150 m long, with polyethene pipes (PE100 PN16) with diameter $\phi = 0.032$ m and wall thickness $h = 0.003$ m, as shown in Fig. 1. This system was directly connected to the water distribution network. A first branch of the system, with a length of about 80 m, was installed between the instrumented pipe system and the water inlet to reduce the influence of noise generated within and transmitted from the water distribution network. The opening of the outlet valve of the pipe system was used to simulate water consumption by any given user at different flow rates. It was possible to replace a segment of the system with a cracked pipe to simulate the presence of a leak in a given position, as shown in the Fig. 1. Preliminary tests were conducted to optimise the test-rig design, involving the simulation of a leak through two distinct damage scenarios on the pipe: a *hole-type* and a *slit-type*. The *hole-type* damage was induced by drilling a hole in the pipe, with a diameter of approximately 2 mm. The *slit-type* damage was created by cutting a 4 cm long slit on the pipe's surface. The *slit-type* leak was chosen to conduct a detailed analysis, as it is more representative of real condition leaks. Besides, the *hole-type* leak also generated a higher level of noise, thereby potentially being less sensitive to noise masking from other sources. Comparison between the acoustic characteristics of the two types of leak is shown in Section 4. Two hydrophones (Aquarian Scientific AS-1[1]) and two water meters were installed in the test rig at positions 26 m apart from each other, denoted as H_1, H_2, WM_1, and WM_2, respectively, as shown in Fig. 1. Hydrophones were preferred over accelerometers due to their suitability for applications in networks with plastic pipes. Nevertheless, the presented methodology is applicable with any vibro-acoustic sensor, provided it allows for a good signal-to-noise ratio. The hydrophones were fitted into the pipe using customised pipe clamp saddles sealed with O-rings, as shown in the pictures provide in Fig. 2. To reduce the effect of the sensors on the water flow, as well as the influence of the water flow on the sensors, the two hydrophones were installed into sub-branches of the test-rig rather than into the main pipe, so they were not directly affected by water flow. Moreover, since the proposed methodology relies on the comparison of spectral characteristics recorded in various conditions, their influence is considered insignificant as it equally affects all conditions. The sensors were connected to a digital audio recorder with a sampling frequency $F_s = 96000$ Hz, which allows for the investigation of a broad range of frequencies (20 Hz – 20 kHz). Although previous studies have found frequency content extending below 20 Hz, this lower range of frequencies is highly susceptible to road traffic vibration. It was therefore considered better to analyse a wider frequency range less affected by this critical masking source in in-situ conditions.

Table 1
Summary of the experimental test conditions.

Cond. ID	flow rate q_i	Condition Description
S_0	$q_l = 0$ l/h $q_{wc} = 0$ l/h	Standard system: at a constant pressure with no flow
S_1	$q_l = 0$ l/h $q_{wc} = 100$ l/h $q_{wc} = 200$ l/h $q_{wc} = 400$ l/h $q_{wc} = 600$ l/h $q_{wc} = 1000$ l/h	Standard system: at a constant pressure with flow due to the opening of the outlet valve (water consumption from users)
L_0	$q_l = 80$ l/h $q_{wc} = 0$ l/h	Leak-system: at a constant pressure with flow due to the presence of a leak
L_1	$q_r = 1.00$ $q_r = 2.13$ $q_r = 5.63$ $q_r = 10.74$ $q_r = 63.50$	Leak-system: flow rate due to the simultaneous presence of a leak and water consumption

Experimental tests and signal acquisition were performed under various conditions to characterise the background noise within the system, the acoustic field generated by a simulated leak, and the noise generated by simulating water consumption. Four main conditions were investigated, each with different flow rates, as summarised in Table 1, where q_{wc} represents the flow rate associated with water consumption, and q_l denotes the flow rate associated with the leak, while their ratio is defined as $q_r = q_{wc}/q_l$. The system in the *standard configuration* with no water flow, denoted as S_0, was analysed to characterise the background noise generated within and transmitted from the water distribution network. On the other hand, S_1 represents the standard configuration of a water distribution network under normal operating conditions, without leaks and with flow due to water consumption from users. The condition L_0 was investigated to acoustically characterise the *leak system*, in which the sound field was generated by the presence of a simulated *slit-type* leak, without any other sound sources except background noise (as characterised in condition S_0). Ultimately, configuration L_1 represents a typical in-situ condition where the noise generated by the leak combines with the noise due to water flow and other sound sources associated with user water consumption. In this latter case, the dif-

[1] range with linear response 1 Hz – 100 kHz (±2 dB), sensitivity 40 μV/Pa.

Fig. 2. Pictures of the two hydrophone fitted in the pipes of test-rig.

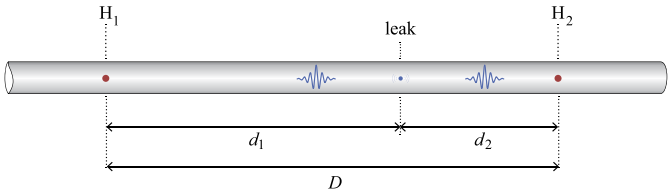

Fig. 3. Diagram of the sensors arrangement for leak localisation through vibroacoustic signals cross-correlation.

ferent conditions of fluid flow, dependent on both the leak and the simulated water consumption, are described in terms of the flow rate ratio q_r, as the flow rate associated with the leak changes along with the flow rate associated with water consumption. To ensure clarity, it is important to specify that the flow rates associated with water consumption in conditions L_1 were near the values obtained in conditions S_1, although not identical. While the sensors in the test-rig provided an accurate measurement of flow rates, manual adjustments made it possible to achieve only comparable rates across different conditions. Additionally, varying water consumption flow rate also affected the water flow associated with the leak. More specifically, the leak water flow rate, initially around $q_l = 80$ l/h in the condition L_0, decreased to $q_l = 20$ l/h as the water consumption flow approached $q_{wc} = 1000$ l/h.

3.2. Acoustic cross-correlation for leak location

Noise correlators estimate the position of a leak by processing two signals acquired by using acoustic (i.e., hydrophones) or vibration sensors (i.e., accelerometers) placed on access points on the pipe on both sides where the leakage is supposed to be located. According to the diagram in Fig. 3 the distance between the position of one sensor and the leak can be determined as:

$$d_1 = \frac{D - c\delta t}{2} \tag{1}$$

where D is the distance measured between the two sensors, c is the propagation velocity of the sound wave generated by the leak along the fluid-filled pipe, and δt is the delay observed in the time of arrival of the perturbance between the two sensor positions H_1 and H_2. As expressed by Eq. (1), the reliability of the leak pinpointing depends on the accuracy of the estimate of both the wave propagation velocity c and the time delay δt, representing the two unknowns whose evaluation is addressed in the following two subsections respectively.

3.2.1. Estimate of wave propagation velocity

The wave propagation velocity along a segment of a water distribution network depends on the dynamic coupling between the pipe's elastic structure and the fluid contained within it. In practical conditions, where the distribution network consists of buried pipes, the interaction between the pipe walls and the surrounding ground should also be considered. Nevertheless, for unburied pipes, such as the test rig built for this study, the effect of the air surrounding the duct is negligible. Thus, the theories of dynamics derived in in-vacuum conditions remain valid. For the study presented here, the wave propagation velocity in unburied fluid-filled pipes was computed using the approximated solutions proposed by Pinnington and Briscoe [19], based on a simplified form of Kennard's equation of motion for circular cylindrical shells [42]. These approximated formulations are valid only well below the pipe ring frequency since they neglect the pipe bending in their derivation. The pipe ring frequency $\omega_R = c_L/a$ occurs when the wavelength of a quasi-longitudinal wave, propagating in a plate-like structure, equals the circumference of the pipe, where a is the pipe radius, and c_L is the longitudinal wave velocity. Considering axisymmetric propagating modes, identified by the circumferential modal order $n = 0$ in the diagrams provided in Fig. 4, three different waves propagate in the system [15]. The predominantly fluid-borne wave ($s = 1$) and the predominantly structure-borne wave ($s = 2$) are quasi-longitudinal waves that induce axial and radial motion of the fluid and the pipe. The torsional wave mode ($s = 0$) is not of particular interest in leak noise applications as it induces negligible radial motion that remains uncoupled from the fluid. The solutions for the wavenumber k_s with $s = 1, 2$ can be expressed as [19]:

$$\begin{cases} k_1^2 = k_0^2 \left(\frac{1+\beta-\nu^2-\Omega^2}{1-\nu^2-\Omega^2} \right) \\ k_2^2 = k_L^2 \left(\frac{1+\beta-\Omega^2}{1+\beta-\nu^2-\Omega^2} \right) \end{cases} \tag{2}$$

where $\Omega = \omega/\omega_R$ is the non-dimensional ring frequency, $k_0 = \omega/c_0$ is the acoustic wavenumber propagating in an infinite fluid medium, and $k_L = \omega/c_L$ is the quasi-longitudinal wavenumber propagating in a plate-like structure, computed from the elastic modulus E of the cylindrical shell, its Poisson's ratio ν, and density ρ as:

$$k_L = \omega \sqrt{\frac{\rho\left(1-\nu^2\right)}{E}} \tag{3}$$

The term β, representing the fluid loading on the pipe structure, is given by:

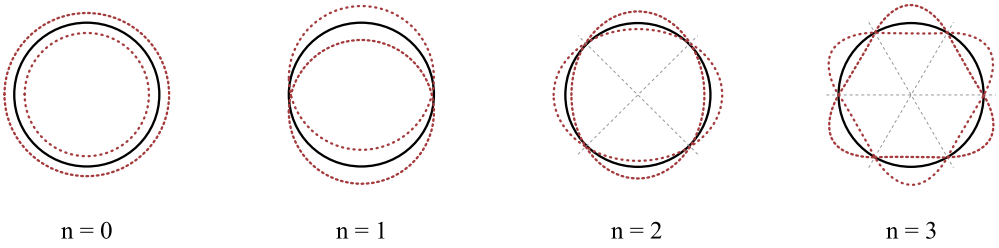

Fig. 4. Diagram of the mode shapes of a cylindrical shell with circumferential modal order up to $n = 3$.

$$\beta = \frac{2Ba}{Eh}\left(1 - \nu^2\right) \tag{4}$$

where h is the pipe wall thickness, and $B = c_0^2\rho_0$ is the fluid bulk modulus, with ρ_0 indicating the fluid density. The term β expresses the effects of the fluid contained in the cylindrical shell on the dynamic of the system. For an empty shell, $\beta = 0$. As β increases, the phase velocity $c_1 = \omega/k_1$ decreases, and the phase velocity $c_2 = \omega/k_2$ tends to the value of c_L. Moreover, the contained fluid limits the radial motion of the elastic structure, making it more difficult to be detected by vibrational transducers for transverse displacement. The predominantly fluid-borne wave mode $s = 1$, responsible for the larger amount of energy propagating due to the leak presence [25], is of most interest in the application of acoustic cross-correlation for leak localization.

An accurate estimate of the wave propagation velocity is fundamental to obtain a reliable position of the leak within the investigated system, as clearly expressed by Eq. (1). It should be noted that, even though in a coupled vibroacoustic system (such as an elastic shell filled with a fluid medium), multiple modes propagate at each frequency with different phase velocities along both the elastic and the acoustic domains [43], the energy content of a sound wave generated due to the presence of a leak in a pipe mainly travels within the system as a predominantly fluid-borne wave (i.e., the branch $s = 1$). An estimate of the wave propagation velocity $c_1 = \omega/k_1$ of the predominantly fluid-borne propagating mode was obtained using Eq. (2) from the characteristics of the pipe's material and the fluid. The experimental test rig was realised using polyethylene pipes (PE100 PN16) with radius a and wall thickness h. The material PE100 constituting the pipes was characterised by elastic constants found in the literature [44], even though its vibroacoustic behaviour would be more accurately described through frequency-dependent elastic properties to account for viscoelastic effects. Table 2 shows the elastic characteristics of PE100, together with the fluid's properties and the pipe's geometry required to compute the wave propagation velocity in the system considered here. Eqs. (2), developed by Pinnington and Briscoe [19], pertain to in-vacuum fluid-filled pipes and frequencies well below ω_R, which is given in Table 2 for the considered system. A comparison between experimental results and the computed phase velocity in-vacuum conditions, as presented by Muggleton et al. [23], demonstrates a good agreement between the measured and predicted wave velocities. The estimate of the wave propagation velocity c_1 is considered reasonably accurate; however, it is not entirely free from uncertainty due to the input data used in Eq. (2). While this approximation remains suitable for the laboratory configurations tested, it is imperative to emphasise that for buried pipes and in-situ conditions, the influence of the surrounding soil on wave propagation velocity cannot be disregarded. However, this influence can be adequately addressed by employing analytical formulations [21,20].

Fig. 5 shows the estimated wavenumbers and phase velocity dispersion curves of the axisymmetric modes propagating in the system, providing the dispersion curves of a wave propagating in an infinite fluid medium (i.e., k_0 and c_0) and in an infinite plate (i.e., k_l and c_L) as a reference. The predominantly fluid-borne wave propagates with a velocity c_1 significantly lower than the propagation velocity c_0 of an acoustic wave in an infinite volume of the same fluid medium. For the sake of completeness, the wavenumber and phase velocity of the predominantly structure-borne wave are also plotted in Fig. 5, showing that the propagation velocity c_2 is similar to the phase velocity of a quasi-longitudinal wave in a plate-like structure c_L.

Table 2
Input data to compute the wave propagation velocity in the considered system.

Pipe Geometry		Fluid Properties		PE100 Characteristics	
a (m)	0.016	c_0 (m)	1480	E (MPa)	1100
h (m)	0.003	ρ_0 (kg/m^3)	1000	ρ (kg/m^3)	950
ω_R (rad/s)	7.47e + 04	β (−)	18.06	ν (−)	0.33

3.2.2. Estimate of time delay

The cross-correlation (CC) approach is a widely used method for estimating the time delay δt between two signals, and it can be implemented in either the time or the frequency domain. Detailed theoretical concepts and implementation requirements can be found in the work of Glentis et al. [45]. Assuming that sensors H_1 and H_2 acquire two stationary continuous signals, denoted as x_1 and x_2 respectively, the cross-correlation function is defined as follows:

$$R_{x_1x_2}(\tau) = E[x_1(t)x_2(t+\tau)] \tag{5}$$

where $E[\cdot]$ represents the expected value operator and τ is the time lag. The time delay is determined by maximising the cross-correlation function: $\delta t = \arg\max_\tau(R_{x_1x_2}(\tau))$. The reliability of the time delay estimate between two signals is significantly affected by background noise. While Eq. (5) provides an intuitive and direct definition of the cross-correlation function, it is more efficiently evaluated in the frequency domain. The cross-correlation function between the signals x_1 and x_2, denoted as $R_{x_1x_2}(\tau)$, is linked to their cross-spectral density (CSD) $S_{x_1x_2}(\omega)$. Specifically, it can be obtained by performing the inverse Fourier transform of $S_{x_1x_2}(\omega)$:

$$R_{x_1x_2}(\tau) = \frac{1}{2\pi}\int_{-\infty}^{\infty} S_{x_1x_2}(\omega)e^{j\omega\tau}\mathrm{d}\omega \tag{6}$$

where $j = \sqrt{-1}$ denotes the imaginary unit. Eq. (6) represents the basic cross-correlation (BCC) used in this study. Gao et al. [29] explored the use of the generalised cross-correlation (GCC) to emphasise the peak in the function by applying a frequency domain weighting function to the CSD before performing the inverse Fourier transform. The results obtained from the computation of the cross-correlation function in this study were implemented using the BCC in the frequency domain within MATLAB®.

Each recorded signal, treated as stationary, was divided into N segments of $n_s = 96000$ samples (equivalent to 1-second time slices).[2] To reduce the impact of random background noise, the cross-correlation function was averaged as:

[2] This averaging approach requires segment lengths longer than the expected delay between the signals [46]. In this case, the minimum segment length was estimated considering the distance between sensors H_1 and H_2: $t_{\min} = D/c \approx 0.083$ s (corresponding to 7975 samples $< n_s$).

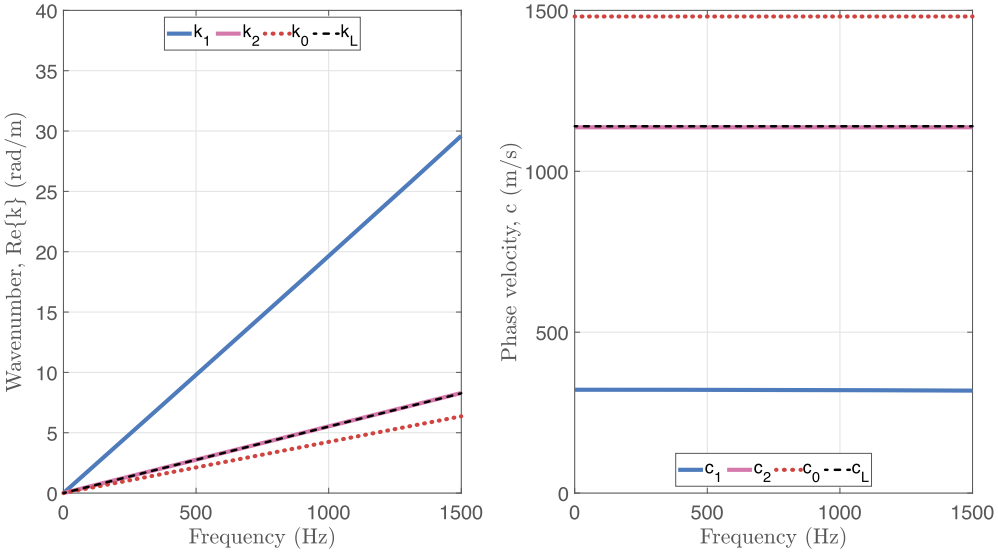

Fig. 5. Estimated dispersion curves of the axisymmetric propagating modes, in terms of wavenumbers (real part) on the left-hand side, in terms of phase velocity of the right-hand side.

$$\bar{R}_{x_1x_2}(\tau) = \frac{1}{N}\sum_{n=1}^{N} R_{x_1x_2}(\tau) \tag{7}$$

The averaging in Eq. (7) helps reducing the effect of non-correlated background noise that may mask the leak signal. However, it is not effective with correlated noise generated within the system, such as noise from water consumption. To improve the accuracy in the time delay estimate, even in the presence of partial noise masking, the recorded signals were pre-filtered using a second-order Butterworth bandpass filter. The cutoff frequencies of the filter were determined through spectral analysis, as detailed in section 4.1.

4. Results and discussion

The following sections present the most significant results obtained from the experimental analysis. Firstly, we introduce the spectral characterisation of the investigated systems, under the different conditions described in Section 3.1. Then, we assess the accuracy of acoustic correlation in locating a leak within the distribution network, both in ideal undisturbed conditions and in the presence of noise masking due to water consumption. Finally, in Section 4.3, we summarise and discuss more in-depth the observed results.

4.1. Acoustic field characterisation

We performed a spectral analysis on the audio signals recorded inside the distribution system to characterise the frequency content of the sound field into the pipes in different tested configurations.

4.1.1. Leak type

Before analysing the results associated with the different operating conditions, Fig. 6 compares the power density spectra (PSD) associated with the two different simulated leaks investigated during preliminary tests, as described in Section 3.1. The measurement condition labelled L_0^* is associated with a leak-system configuration with no water consumption. The superscript * is used to indicate that the test-rig configuration is not exactly the same one used in the further analyses, illustrated in Fig. 1, as these tests were performed in a preliminary stage to define the most adequate test-rig set-up. However, the primary difference between the two systems lies in the length of the pipe that connects the test rig to the principal water distribution network. This difference, as discussed in the next section, affects the transmission of low-frequency background noise originating from the principal water distribution network, equally impacting both leak simulations. Furthermore, the various conditions assessed in the preliminary test-rig are characterised in relation to the global flow rate, due to the absence of additional sensors to differentiate between the flow rate associated with water consumption and that associated with the leak. Fig. 6 compares the sound pressure level spectra generate by a *hole-type*, denoted as $H_{i,L_0^*,HOLE}$, leak and a *slit-type* leak, denoted as $H_{i,L_0^*,SLIT}$, at the same flow rate. This comparison highlights significantly higher sound pressure levels[3] generated with a *hole-type* leak in both the sensor positions across the entire investigated frequency range, which makes the *slit-type* leak noise more sensitive to noise masking by other sound sources. In the same graphs the background noise of the system in the absence of flow is denoted as H_{i,S_0^*}. In position H_1, this background noise reaches, and in some cases exceeds, the sound pressure level generated by the *slit-type* leak across almost within the entire investigated frequency range. Modifications were implemented on the test-rig to attenuate the noise transmitted from the water supply network, as described in Section 3. We chose to conduct a detailed analysis using the *slit-type* leak in the optimised test-rig, as presented in the following sections. This choice was motivated by its greater susceptibility to masking effects. Additionally, this form of pipe damage more accurately mirrors real-world, in-situ conditions.

4.1.2. Leak generated noise

The sound field generated in the test-rig under condition L_0 was analysed to characterise the spectra components associated with the perturbance generated by the presence of a (*slit-type*) simulated leak. As shown in Fig. 7, the spectra associated with the noise generated by the leak, identified as H_{i,L_0}, predominantly exhibit low-frequency components, between 20 Hz and 100 Hz, although its energy content extends across a wide frequency range, up to 3000 Hz. In the same Figure, the noise generated by the leak spectra is compared to the background noise of the system, characterised under condition S_0, where no water flow was present in the test-rig. The comparison reveals a similar trend, with a predominance of low-frequency components in the background noise spectra, indicated as H_{i,S_0}. However, the sound field generated due to the presence of the simulated leak exhibits higher sound pressure levels than the background noise up to approximately 3000 Hz at position

[3] The magnitude of the spectra, expressed as sound pressure levels referred to $p_0 = 1$ μPa, was used only for relative comparisons.

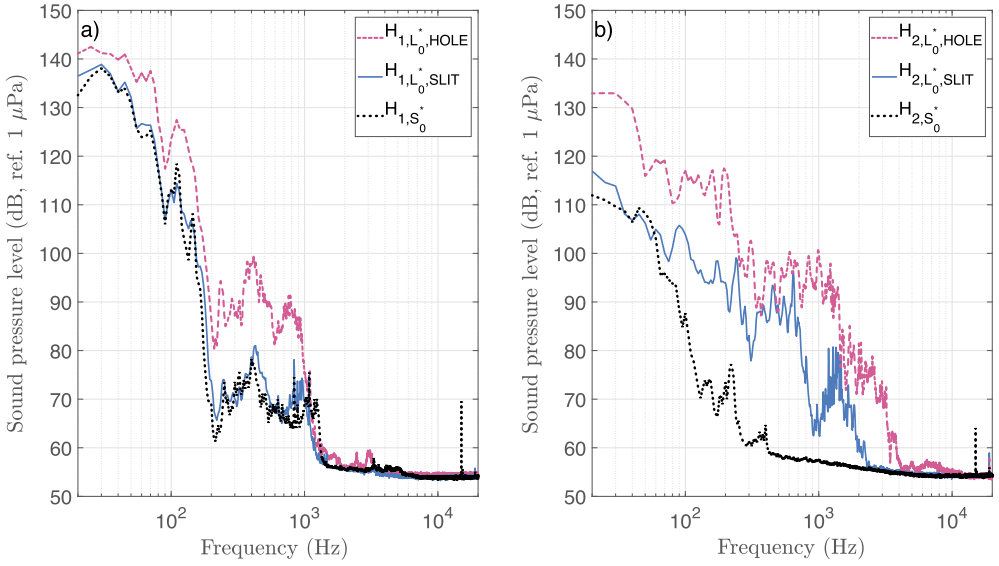

Fig. 6. Narrow band sound pressure level spectra measured in the conditions S_0^* and L_0^* with two different simulated leaks, *slit-type* and *hole-type* leak: a) hydrophone H_1 (upstream); b) hydrophone H_2 (downstream).

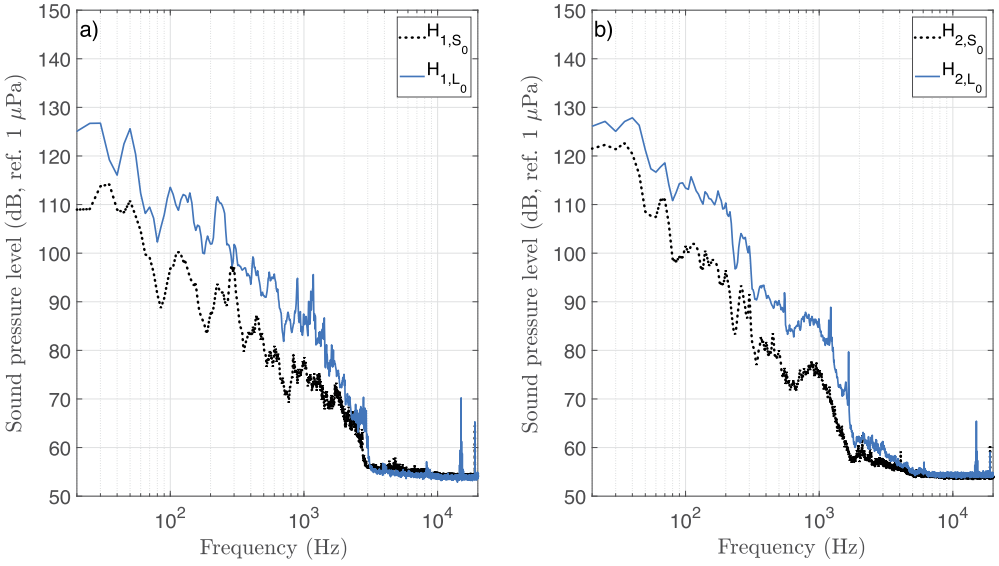

Fig. 7. Narrow band sound pressure level spectra measured in the conditions S_0 and L_0: a) hydrophone H_1 (upstream); b) hydrophone H_2 (downstream).

H_1 and 2000 Hz at position H_2. As indicated by the subscript $_0$, in both these conditions, the outlet valve of the test-rig, simulating water consumption from users, was closed. In condition S_0, there was no water flow in the system, while in condition L_0, a flow rate $q_l \approx 80$ l/h due to the leak was measured. In the next paragraph, the possible masking of the leak sound wave due to the noise generated by water consumption is analysed, by comparing the sound spectra associated with the simultaneous presence of a leak and water consumption, to the noise leak characteristic spectra illustrated in this section.

4.1.3. Noise masking

The operating conditions, identified as S_1, were analysed to characterise the sound field generated in a leak-free system due to water consumption from users at different flow rates. While in the mixed conditions L_1, different flow rates were investigated in the simultaneous presence of water consumption and a leak in the system. Each configuration is characterised in terms of the flow rate ratio $q_r = q_{wc}/q_l$ between the flow rate associated with water consumption q_{wc} and the flow associated with the leak q_l.

To assess the potential masking of the leak disturbance by water consumption noise, Fig. 8 compares the sound pressure level spectra obtained in the condition L_1 with a flow rate ratio $q_r \approx 1.00$ with the characteristic sound pressure level spectra associated with the condition L_0. The mixed condition, denoted as $H_{i,L_{1,q_r\ 1.00}}$, exhibits lower sound pressure levels compared to the condition L_0, where the acoustic disturbance was only due to the leak (H_{i,L_0}), at least up to approximately 550 Hz in position H_1 and within a broader frequency range in position H_2. Besides, to highlight potential noise masking and how the presence of the leak affects the sound field due to water consumption, the sound pressure level spectra measured in condition S_1 for a flow rate $q_{wc} \approx 100$ l/h due to water consumption alone are also provided ($H_{i,S_{q_{wc}100}}$). In position H_1 above 300 Hz, the spectra associated with condition L_1 exhibit significantly higher sound pressure levels than the spectra measured in the absence of a leak in condition S_1. Smaller differences can be observed between these two conditions in

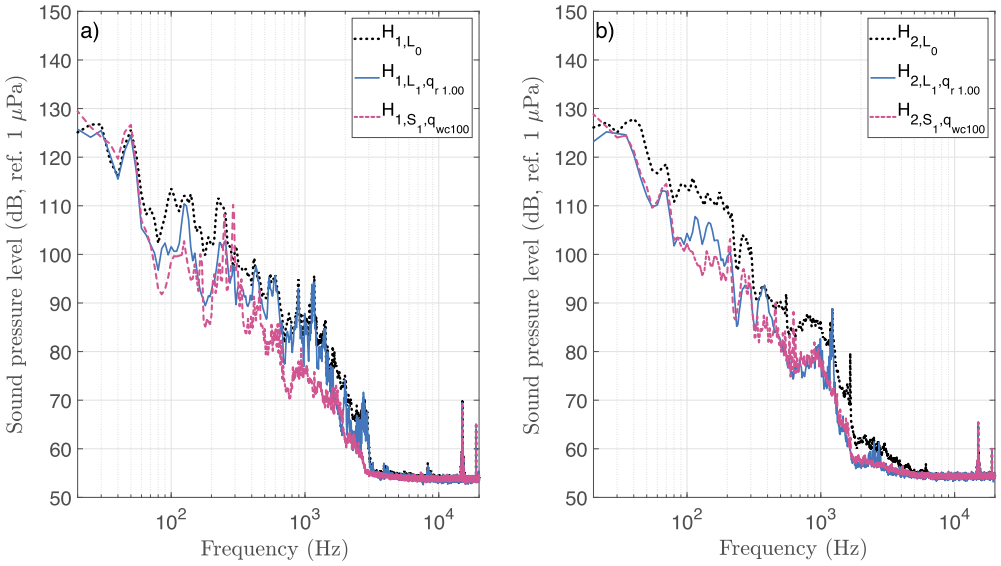

Fig. 8. Narrow band sound pressure level spectra measured in the conditions L_0 (leak only), S_1 (water consumption $q_{wc} \approx 100$ l/h) and L_1 (mixed water flow $q_r \approx 1.00$): a) hydrophone H_1 (upstream); b) hydrophone H_2 (downstream).

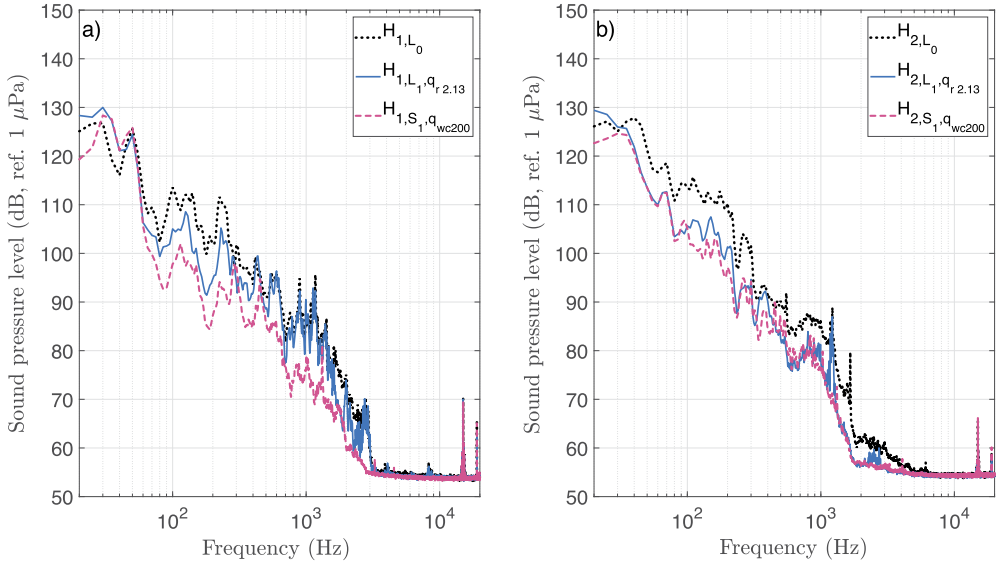

Fig. 9. Narrow band sound pressure level spectra measured in the conditions L_0 (leak only), S_1 (water consumption $q_{wc} \approx 200$ l/h) and L_1 (mixed water flow $q_r \approx 2.13$): a) hydrophone H_1 (upstream); b) hydrophone H_2 (downstream).

position H_2, which is closer to the system outlet. The characteristic sound pressure level spectra of the mixed condition $H_{2,L_{1,q_r\ 1.00}}$ have a higher amplitude than the spectra associated to water consumption $H_{2,S_{q_{wc}100}}$ only within the frequency ranges 90 Hz – 200 Hz and 300 Hz – 450 Hz. The comparison of the average spectra in Fig. 8, characterised by a low, and sometime negative, signal-to-noise ratio defined as $\mathrm{SNR}_1 = H_{i,L_{1,q_{r_j}}} - H_{i,S_{1,q_{wc_j}}}$, highlights a potential partial masking of the sound field generated by the leak.

A more in-depth investigation, comparing the spectra associated with the testing conditions S_1 and L_1 for different values of the flow rate ratio q_r, allows for the identification of the frequency range less affected by the masking of the leak-generated noise. The sound pressure level spectra associated with flow rate ratios $q_r = 2.13$ and $q_r = 10.74$ are compared in Fig. 9 and Fig. 10, respectively. The general observations discussed concerning the spectra associated with a flow rate ratio $q_r = 1.00$, shown in Fig. 8, can be extended to higher flow rate ratios. Moreover, it can be noted that as the flow rate associated with water consumption increases, the frequency range affected by possible noise masking broadens, especially in position H_1. Even up to a flow rate ratio of approximately $q_r \approx 10.74$, the observed sound pressure levels associated with the L_1 condition are slightly higher than the sound pressure levels associated with the S_1 condition in both measurement positions, within the frequency range between 300 Hz and 500 Hz. However, when considering higher flow rate ratios, the results highlight a complete masking effect. The term *"partial masking"* describes a condition in which, within the range of interest, there are specific frequency bands with $\mathrm{SNR}_1 > 1$. On the other hand, the *complete masking* condition occurs when $\mathrm{SNR}_1 \leq 0$ across the entire investigated frequency range. This is shown for a flow rate $q_r = 63.50$ in Fig. 11, where the sound pressure level spectra in position H_2 associated with the mixed operating condition, denoted as $H_{2,L_{1,q_{r63.50}}}$, exhibit a lower amplitude than the spectra associated with the condition S_1, denoted as $H_{2,S_{q_{wc}1000}}$, across the entire frequency range.

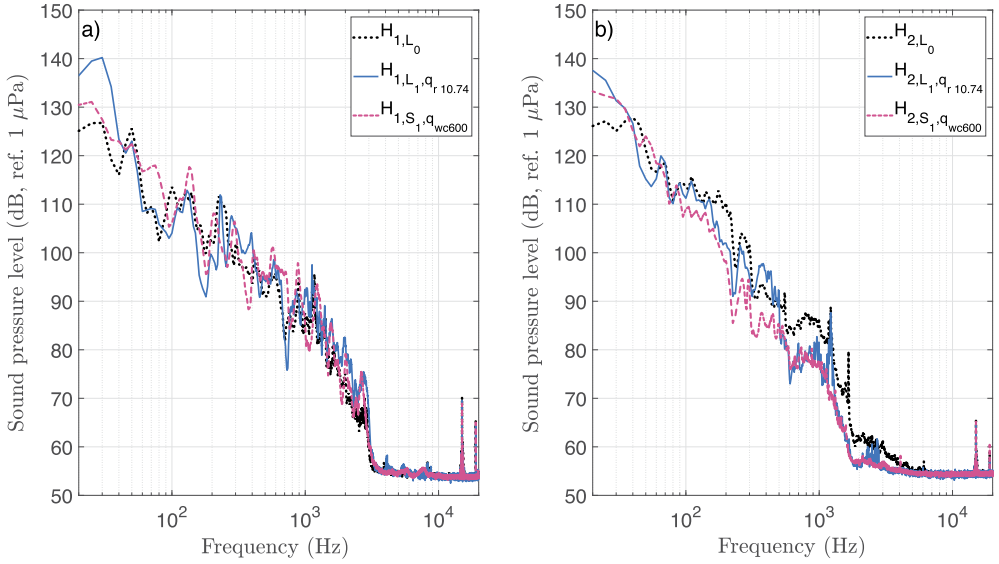

Fig. 10. Narrow band sound pressure level spectra measured in the conditions L_0 (leak only), S_1 (water consumption $q_{wc} \approx 600$ l/h) and L_1 (mixed water flow $q_r \approx 10.74$): a) hydrophone H_1 (upstream); b) hydrophone H_2 (downstream).

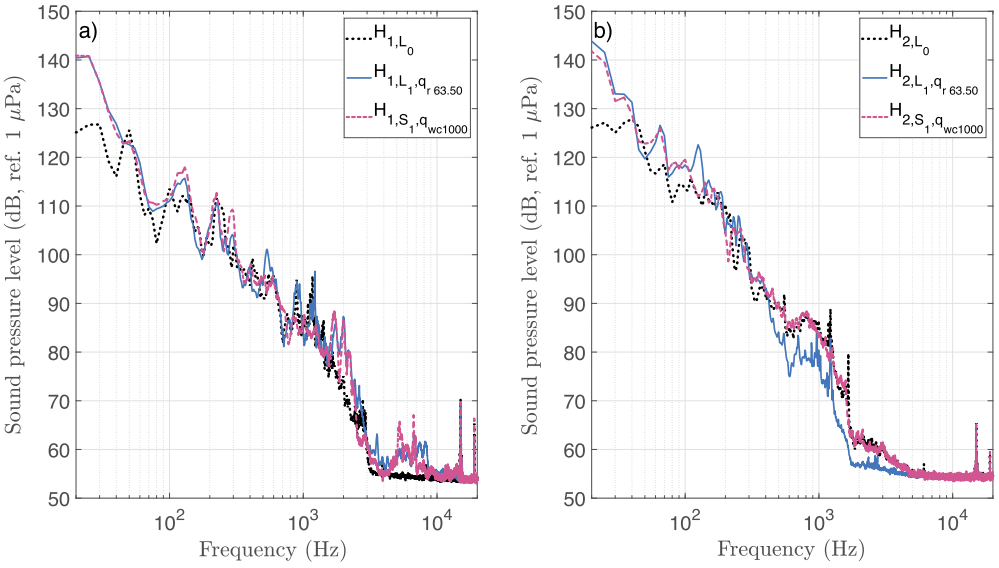

Fig. 11. Narrow band sound pressure level spectra measured in the conditions L_0 (leak only), S_1 (water consumption $q_{wc} \approx 1000$ l/h) and L_1 (mixed water flow $q_r \approx 63.50$): a) hydrophone H_1 (upstream); b) hydrophone H_2 (downstream).

As demonstrated in the next section, the influence of partial masking could be significantly reduced by using a 2nd-order Butterworth band-pass filter with a lower cut-off frequency of 300 Hz and an upper cut-off frequency of 500 Hz. However, in cases of total masking, using recorded signals for acoustic leak location is not feasible.

4.2. Leak location

The signals recorded at positions H_1 and H_2 in different test-rig conditions are used to localise the leak using the acoustic correlation approach described in Section 3.2. For each testing condition, the time delay estimate $\delta\bar{t}$ is determined by maximising the cross-correlation function of the two recorded signals. The distance between the sensor H_1 and the position of the simulated leak is estimated using Equation (1). The results are summarised in Table 3. Condition L_0 represents the quietest condition, with minimal masking limited to the background noise transmitted from the water distribution network. For each condition L_1 associated with a different ratio between the leak and water consumption flow rates, q_r, Table 3 provides the leak location estimates obtained with and without pre-filtering the signals. The error estimate was evaluated as $\varepsilon = |\bar{d} - d|/d$, where $\bar{d}$ is the estimated distance and $d = 23$ m is the expected distance. It should be noted that even in the optimal measurement condition, an error of $\varepsilon \approx 8\%$ of the nominal distance was observed. This can be caused by uncertainties in the measured expected distance (due to the presence of bends or T-junctions), uncertainties in the evaluation of the time delay, and uncertainties in the estimated wave propagation velocity, as mentioned in Section 3.2. The results presented here highlight how a noise source unrelated to the leak, such as water consumption from users in the proximity of the investigated segment of the network, can significantly affect the results of the acoustic correlator, leading to a wrong location. However, it is possible to significantly reduce the masking effects of other noise sources by pre-filtering the signals in a suitable frequency range before performing the cross-correlation. This can provide a good SNR_1 in the frequency range of interest for the leak-generated noise and a good approximation of the leak location. To successfully reduce the masking effect and ob-

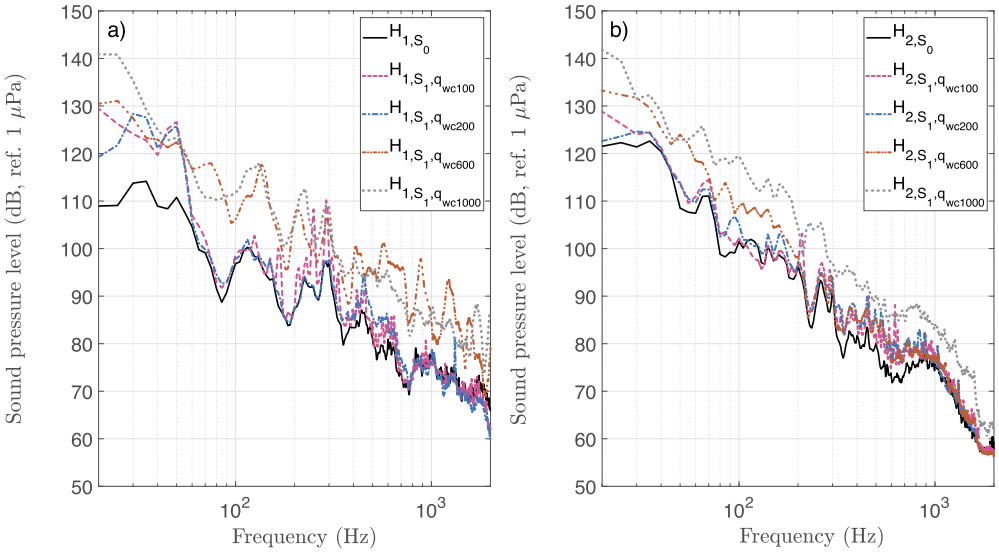

Fig. 12. Narrow band sound pressure level spectra measured in the conditions S_0 (background noise), S_1 (water consumption at different flow rates q_{wc}): a) hydrophone H_1 (upstream); b) hydrophone H_2 (downstream).

Table 3
Estimated distance $\tilde{d}$ from acoustic cross-correlation method: *slit-type* leak under different operating conditions.

Cond. ID	q_r (–)	c_1 (m/s)	n. samples	processing	$\tilde{d}$ (m)	ε (%)
L_0	-	313	4.32e + 06	-	21.0	8.9
				pre-filtering	21.1	8.4
L_1	1.00	313	4.32e + 06	-	−5.9	125.4
				pre-filtering	21.1	8.4
	2.13		4.80e + 06	-	11.0	52.4
				pre-filtering	21.1	8.5
	5.63		3.86e + 06	-	0.2	99.1
				pre-filtering	20.4	11.3
	10.74		5.89e + 06	-	0.7	97.0
				pre-filtering	0.9	96.3
	63.50		5.89e + 06	-	2.2	90.7
				pre-filtering	3.4	85.2

Table 4
Estimated distance $\tilde{d}$ from acoustic cross-correlation method: comparison between *slit-type* and *hole-type* leak under different operating conditions.

Cond. ID	q_t (l/h)	c_1 (m/s)	n. samples	processing	$\tilde{d}$ (m)	ε (%)
$L^*_{0,SLIT}$	–	313	3.84e + 06	-	21.4	7.0
$L^*_{0,HOLE}$	–		3.84e + 06	-	22.4	2.6
$L^*_{1,SLIT,150}$	150	313	1.92e + 06	-	−19.0	182.7
				pre-filtering	24.7	7.3
$L^*_{1,HOLE,150}$	150		3.84e + 06	-	37.1	60.2
				pre-filtering	21.9	4.7
$L^*_{1,SLIT,650}$	650		2.76e + 06	-	21.6	6.0
				pre-filtering	23.5	2.4
$L^*_{1,HOLE,650}$	650		2.76e + 06	-	26.6	15.9
				pre-filtering	23.7	2.9

tain reliable results, it is essential to define the characteristics of the bandpass filter, based on a spectral analysis of the acoustic field that characterises the system. This allows for discrimination between the signal of interest and the masking sources. The findings of the experimental analysis showed that for a flow rate ratio up to $q_r = 5.63$, the leak can be located with an error of approximately $\varepsilon = 11\%$ of the nominal distance (only slightly higher than the error observed in the ideal condition L_0, $\varepsilon \approx 8\%$). It is worth noting that even though the spectra associated with condition L_1 : $q_r = 10.74$, shown in Fig. 10, apparently exhibit higher levels than the spectra associated with S_1 : $q_{wc} = 600$ within the range of interest that could be associated with the leak noise, the pre-filtering does not preempt the effect of noise masking. In fact, the acoustic correlator fails to locate the leak with water consumption flow rates ratios equal to or higher than $q_r = 10.74$.

Finally, the effectiveness of the proposed pre-filtering, using the same filter set-up, is analysed comparing the different simulated leaks, tested during a preliminary phase of this study. Results of leak location estimates, for different operating conditions characterised in terms of total flow rate q_t, obtained with both a *hole-type* leak and a *slit-type* leak are summarised Table 4. Analogously to results presented in Table 3, when the leak is the only source of noise, pre-filtering is not necessary and the noise correlation approach provides a good approximation of the leak location with both simulated leaks. On the other hand, when the noise generated by the leak combines with noise generated by water consumption, signal pre-filtering is necessary in order to locate the leak with good accuracy. For all the tested conditions, the location of the *hole-type* leak was located with higher accuracy, both with and without pre-filtering. Consistent with the results presented in Section 4.1, the *slit-type* leak noise, having a lower amplitude, is more sensitive to masking by other sound sources.

4.3. Discussion

The spectral analysis of the signals recorded within the laboratory distribution system under different conditions aims to characterise the influence of water flow on the sound field into the pipes and to evaluate the feasibility of distinguishing between acoustic disturbances caused by leaks and the background noise generated by the system, as well as the sound field resulting from water consumption. Under the standard condition S_0, where no leaks, water consumption near the sensors, or other extraneous sound sources are present, the sound field within the pipe is primarily characterised by frequency components below 100 Hz, aligning with findings from previous studies. The noise generated by simulated water consumption exhibits a dependence on the water flow rate, albeit not following a linear relationship. This trend is evident from the sound spectrum levels illustrated in Fig. 12, which compares various leak-free conditions. To enhance readability, the spectra are presented within the frequency range from 100 Hz to 2000 Hz, which is of utmost relevance for the analysis presented here. Across all testing conditions S_1, with a non-zero water flow rate q_{wc}, higher sound pressure levels are observed compared to the standard condition S_0. As the water flow rates increase from $q_{wc} = 100$ l/h to $q_{wc} = 200$ l/h, no substantial differences are observed in the spectra characterising the sound field at

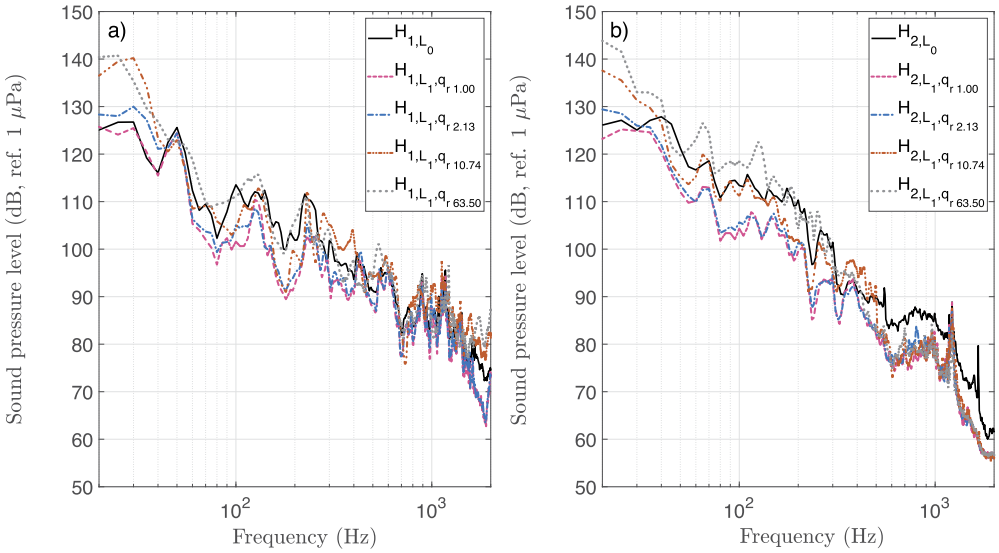

Fig. 13. Narrow band sound pressure level spectra measured in the conditions L_0 (leak only), L_1 (mixed water flow at different flow rate ratios q_r): a) hydrophone H_1 (upstream); b) hydrophone H_2 (downstream).

positions H_1 and H_2. However, rising the water consumption flow rates to $q_{wc} = 600$ l/h, sound pressure levels measured at position H_1 considerably increase. Further increasing of the flow rates leads to higher sound pressure levels also at position H_2.

To analyse how the flow rate due to water consumption combined with a leak in the system affects the sound field, Fig. 13 shows the sound pressure level spectra associated with different conditions of the leak-system. A leak in the system due to a cracked pipe increased the sound pressure level within a wide range of frequencies, from the very low frequencies up to approximately 3000 Hz. The higher-level spectra were measured in condition L_0, where the water flow was only due to the presence of the leak. Even though this seems counter-intuitive, a reduction in the sound pressure levels across the entire range of frequencies was observed by increasing the flow rates associated with water consumption, as highlighted by the spectra associated with conditions L_1. Although this phenomenon is interesting and worthy of further investigation, the understanding of the physical reasons that can explain the acoustic behaviour is beyond the scope of this study. However, it should be noticed that sound pressure levels with higher amplitudes than the spectra L_0 are observed at position H_1 with flow rate ratios $q_r \geq 10.74$, and at position H_2 with $q_r = 63.50$, consistently with the findings presented in Fig. 12.

Finally, the effect of water consumption flow rate on leak pinpointing is further analysed for different operating conditions. Fig. 14 shows the cross-correlation functions between signals recorded at positions H_1 and H_2 under different testing conditions. On the left-hand side, functions obtained by cross-correlating raw signals are shown, while the results on the right-hand side refer to pre-filtered signals. The pair of graphs at the top, associated with condition L_0, and the pair at the bottom, associated with condition S_1, represent two limiting situations. In the first one, the effect of spurious sound sources is minimised, and the cross-correlation functions exhibit the same maximum peak both with and without pre-filtering. In the latter condition, on the other hand, the recorded signals are generated by water consumption with no leak present in the system. In this case, different time delay estimates $\delta\bar{t}$ are obtained with and without pre-filtering the signals. As expected, in both cases the estimate is not consistent with the value expected in the presence of the leak. By comparing the first two graphs on the top left side, associated with unfiltered conditions L_0 and $L_1, q_r = 2.13$ respectively, it is evident how a minimum flow rate not related to the leak could generate frequency components in the recorded signals that may mask the leak sound wave. This results in a maximum peak in the cross-correlation function that does not represent the sought time delay, related to the leak position. However, up to a flow rate ratio $q_r = 2.13$, pre-filtering the signals significantly reduces the masking effect, as shown by the sharp peak in Fig. 14f) (the cross marker indicates the peak amplitude). Maximising the cross-correlation function of pre-filtered signals provides the same time delay estimate $\delta\bar{t}$ found in condition L_0. For higher flow rates, Fig. 14 shows how both with and without signal pre-filtering, the cross-correlation function exhibits multiple peaks, whose maximum is not associated with the leak position. This indicates that the noise generated by water consumption introduces frequency components masking the leak noise even within the band-pass range of the filter, making the pre-processing ineffective.

5. Conclusions

This study conducted a comprehensive characterisation of the acoustic sound field within a pipeline system under varying water flow rates, aiming to distinguish between sound waves generated by leaks in a water distribution system and masking noise arising, for instance, from water consumption by users.

Initially, the spectral characteristics of two simulated leak types, namely the *slit-type* and *hole-type* leaks, were compared. While both leak types predominantly exhibited low-frequency components between 20 Hz and 100 Hz, their spectra extended across a broader frequency range up to approximately 3000 Hz. The *slit-type* leak exhibited lower sound pressure levels when compared to the *hole-type* leak, making it more susceptible to noise masking. For this reason, the subsequent analyses focused on the *slit-type* leak.

The acoustic field generated within the pipes due to simulated water consumption exhibited a non-linear dependency on the water flow rate. Sound pressure levels demonstrated an increase between 20 Hz and 2000 Hz for higher flow rates. Spectra from mixed conditions, involving the simultaneous presence of water consumption and a leak within the system, were analysed to assess the potential masking of the leak disturbance with water consumption noise.

Noise masking notably compromised the accuracy of leak localization through the cross-correlation technique. However, signal pre-filtering, employing the frequency range identified through spectral analysis across different conditions, effectively mitigated the masking effect. This pre-filtering enabled accurate leak localization even in the presence of noise from water consumption. Nonetheless, the effectiveness of pre-filtering was verified up to a threshold flow rate ratio. Above

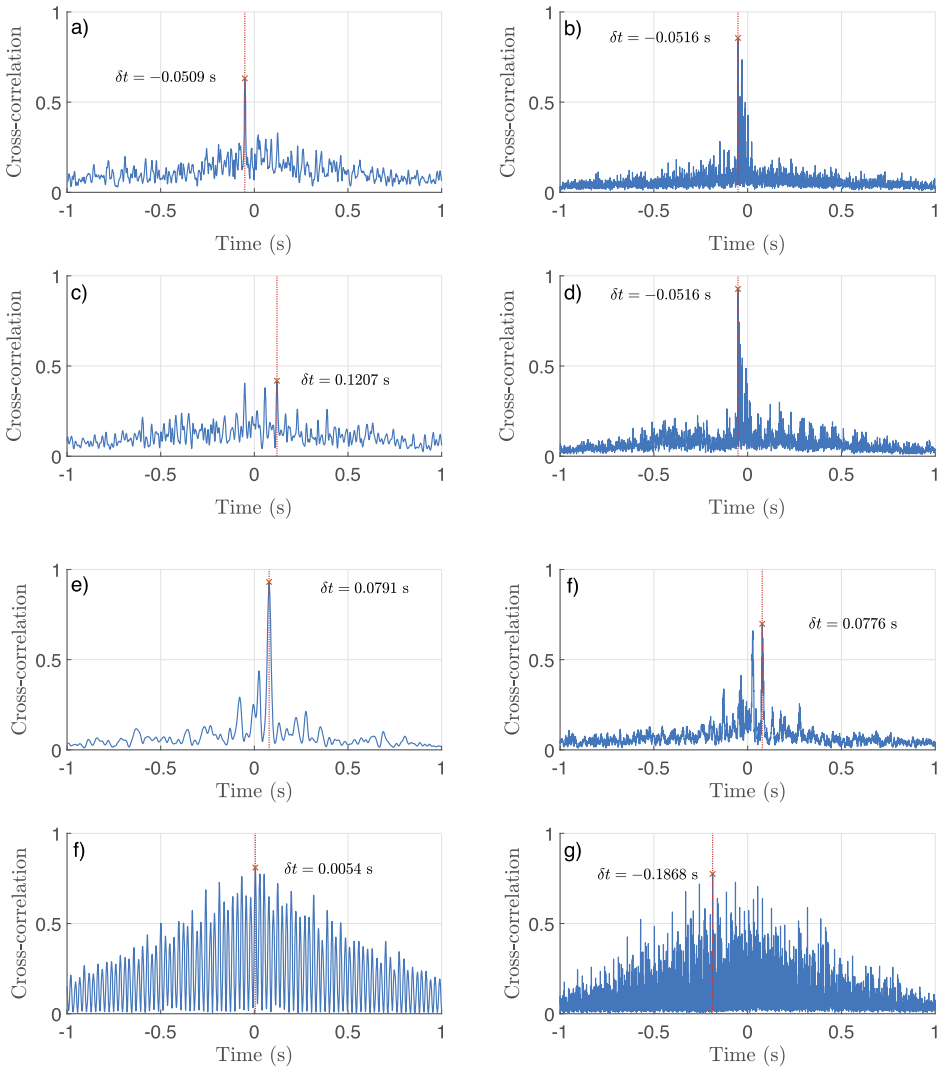

Fig. 14. Examples of cross-correlation functions: L_0: a) unfiltered, b) band pass filtered; $L_1, q_r = 1.00$: c) unfiltered, d) band pass filtered; $L_1, q_r = 2.13$: e) unfiltered, f) band pass filtered; $L_1, q_r = 10.63$: g) unfiltered, h) band pass filtered; $S_1, q_{wc} = 100$ l/h: i) unfiltered, j) band pass filtered.

such threshold, frequency components generated by water consumption prevented an accurate leak location, rendering the filter ineffective even within the designated band-pass range.

The frequency bands and flow rates identified in this study and detailed in the results are specific to the laboratory test rig's geometry and may not universally represent in-situ conditions. Although this study does not introduce novel signal processing methodologies, it does present a systematic methodological framework for characterising the acoustic field generated by diverse sound sources within a water distribution network segment. This approach offers potential for signal pre-filtering in correlation-based leak pinpointing techniques. Despite the controlled laboratory environment of the experimental analyses, this proposed approach could be iteratively applied in-situ by water utility companies, especially considering the potential widespread integration of low-cost vibroacoustic sensors within water distribution networks. This integration stands to significantly enhance leak detection accuracy.

Declaration of competing interest

The authors declare that they have no known competing financial interests or personal relationships that could have appeared to influence the work reported in this paper.

Data availability

The authors are unable or have chosen not to specify which data has been used.

Acknowledgements

The authors would like to express gratitude to the people who have been working on the project WATER 4.0 - Industry 4.0 for Water loss Assessment Through Environmental Research - funded by MiSE - Italian Ministry of Economic Development - in November 2018.

References

[1] Europe's water in figures. An overview of the European drinking water and waste water sectors. EurEau; 2021.
[2] EurEau Briefing note on drinking water supply and leakage management. EurEau; 2021.
[3] Hunaidi O, Chu W, Wang A, Guan W. Detecting leaks in plastic pipes. J Am Water Works Assoc 2000;92(2):82–94. https://doi.org/10.1002/j.1551-8833.2000.tb08819.x.
[4] Liu Z, Kleiner Y. State of the art review of inspection technologies for condition assessment of water pipes. Measurement 2013;46(1):1–15. https://doi.org/10.1016/j.measurement.2012.05.032.
[5] us Saqib N, Mysorewala MF, Cheded L. A multiscale approach to leak detection and localization in water pipeline network. Water Resour Manag 2017;31(12):3829–42. https://doi.org/10.1007/s11269-017-1709-3.

[6] El-Zahab S, Zayed T. Leak detection in water distribution networks: an introductory overview. Smart Water 2019;4(1):1–23. https://doi.org/10.1186/s40713-019-0017-x.
[7] Ben-Mansour R, Habib M, Khalifa A, Youcef-Toumi K, Chatzigeorgiou D. Computational fluid dynamic simulation of small leaks in water pipelines for direct leak pressure transduction. Comput Fluids 2012;57:110–23. https://doi.org/10.1016/j.compfluid.2011.12.016.
[8] Hamilton S, Charalambous B. Leak detection: technology and implementation. IWA Publishing; 2013.
[9] Fuchs HV, Riehle R. Ten years of experience with leak detection by acoustic signal analysis. Appl Acoust 1991;33(1):1–19. https://doi.org/10.1016/0003-682X(91)90062-J.
[10] Fantozzi M, Di Chirico G, Fontana E, Tonolini F. Leak inspection on water pipelines by acoustic emission with cross-correlation method. In: Annual conference proceeding, American water works association, engineering and operations; 1993. p. 609–21.
[11] Puust R, Kapelan Z, Savic D, Koppel T. A review of methods for leakage management in pipe networks. Urban Water J 2010;7(1):25–45. https://doi.org/10.1080/15730621003610878.
[12] Hunaidi O, Chu WT. Acoustical characteristics of leak signals in plastic water distribution pipes. Appl Acoust 1999;58(3):235–54. https://doi.org/10.1016/S0003-682X(99)00013-4.
[13] Brennan M, Karimi M, Almeida F, De Lima FK, Ayala P, Obata D, et al. On the role of vibro-acoustics in leak detection for plastic water distribution pipes. Proc Eng 2017;199:1350–5. https://doi.org/10.1016/j.proeng.2017.09.350.
[14] Lin T, Morgan G. Wave propagation through fluid contained in a cylindrical, elastic shell. J Acoust Soc Am 1956;28(6):1165–76. https://doi.org/10.1121/1.1908583.
[15] Fuller C, Fahy FJ. Characteristics of wave propagation and energy distributions in cylindrical elastic shells filled with fluid. J Sound Vib 1982;81(4):501–18. https://doi.org/10.1016/0022-460X(82)90293-0.
[16] Photiadis DM. The propagation of axisymmetric waves on a fluid-loaded cylindrical shell. J Acoust Soc Am 1990;88(1):239–50. https://doi.org/10.1121/1.400348.
[17] Sinha BK, Plona TJ, Kostek S, Chang S-K. Axisymmetric wave propagation in fluid-loaded cylindrical shells. I: theory. J Acoust Soc Am 1992;92(2):1132–43. https://doi.org/10.1121/1.404040.
[18] Plona TJ, Sinha BK, Kostek S, Chang S-K. Axisymmetric wave propagation in fluid-loaded cylindrical shells. II: theory versus experiment. J Acoust Soc Am 1992;92(2):1144–55. https://doi.org/10.1121/1.404041.
[19] Pinnington R, Briscoe A. Externally applied sensor for axisymmetric waves in a fluid filled pipe. J Sound Vib 1994;173(4):503–16. https://doi.org/10.1006/jsvi.1994.1243.
[20] Muggleton J, Brennan M, Pinnington R. Wavenumber prediction of waves in buried pipes for water leak detection. J Sound Vib 2002;249(5):939–54. https://doi.org/10.1006/jsvi.2001.3881.
[21] Gao Y, Sui F, Muggleton JM, Yang J. Simplified dispersion relationships for fluid-dominated axisymmetric wave motion in buried fluid-filled pipes. J Sound Vib 2016;375:386–402. https://doi.org/10.1016/j.jsv.2016.04.012.
[22] Brennan MJ, Almeida FLCd, Lima FKd, Castillo PCA, Paschoalini AT. Measurement of the speed of leak noise propagation in buried water pipes: challenges and difficulties. In: International symposium on dynamic problems of mechanics. Springer; 2017. p. 511–22.
[23] Muggleton J, Brennan M, Linford P. Axisymmetric wave propagation in fluid-filled pipes: wavenumber measurements in in vacuo and buried pipes. J Sound Vib 2004;270(1–2):171–90. https://doi.org/10.1016/S0022-460X(03)00489-9.
[24] Gao Y, Brennan M, Joseph P, Muggleton J, Hunaidi O. On the selection of acoustic/vibration sensors for leak detection in plastic water pipes. J Sound Vib 2005;283(3–5):927–41. https://doi.org/10.1016/j.jsv.2004.05.004.
[25] Gao Y, Brennan MJ, Joseph PF, Muggleton JM, Hunaidi O. A model of the correlation function of leak noise in buried plastic pipes. J Sound Vib 2004;277(1–2):133–48. https://doi.org/10.1016/j.jsv.2003.08.045.
[26] Almeida F, Brennan M, Joseph P, Whitfield S, Dray S, Paschoalini A. On the acoustic filtering of the pipe and sensor in a buried plastic water pipe and its effect on leak detection: an experimental investigation. Sensors 2014;14(3):5595–610. https://doi.org/10.3390/s140305595.
[27] Brennan M, De Lima FK, De Almeida F, Joseph P, Paschoalini A. A virtual pipe rig for testing acoustic leak detection correlators: proof of concept. Appl Acoust 2016;102:137–45. https://doi.org/10.1016/j.apacoust.2015.09.015.
[28] Brennan MJ, Gao Y, Joseph PF. On the relationship between time and frequency domain methods in time delay estimation for leak detection in water distribution pipes. J Sound Vib 2007;304(1–2):213–23. https://doi.org/10.1016/j.jsv.2007.02.023.
[29] Gao Y, Brennan MJ, Joseph PF. A comparison of time delay estimators for the detection of leak noise signals in plastic water distribution pipes. J Sound Vib 2006;292(3–5):552–70. https://doi.org/10.1016/j.jsv.2005.08.014.
[30] Ahadi M, Bakhtiar MS. Leak detection in water-filled plastic pipes through the application of tuned wavelet transforms to acoustic emission signals. Appl Acoust 2010;71(7):634–9. https://doi.org/10.1016/j.apacoust.2010.02.006.
[31] Zhong Z, Suzuki J, Miyake T, Kondou H, Enastu K. Study on water leak detection using wavelet instantaneous cross-correlation. In: 2015 international conference on wavelet analysis and pattern recognition (ICWAPR). IEEE; 2015. p. 133–7.
[32] Bentoumi M, Chikouche D, Mezache A, Bakhti H. Wavelet DT method for water leak-detection using a vibration sensor: an experimental analysis. IET Signal Process 2017;11(4):396–405. https://doi.org/10.1049/iet-spr.2016.0113.
[33] Ting L, Tey J, Tan A, King Y, Faidz A. Improvement of acoustic water leak detection based on dual tree complex wavelet transform-correlation method. IOP conference series: Earth and environmental science, vol. 268. IOP Publishing; 2019. p. 012025.
[34] Chan TK, Chin CS, Zhong X. Review of current technologies and proposed intelligent methodologies for water distributed network leakage detection. IEEE Access 2018;6:78846–67. https://doi.org/10.1109/ACCESS.2018.2885444.
[35] Banjara NK, Sasmal S, Voggu S. Machine learning supported acoustic emission technique for leakage detection in pipelines. Int J Press Vessels Piping 2020;188:104243. https://doi.org/10.1016/j.ijpvp.2020.104243.
[36] da Cruz RP, da Silva FV, Fileti AMF. Machine learning and acoustic method applied to leak detection and location in low-pressure gas pipelines. Clean Technol Environ Policy 2020;22:627–38. https://doi.org/10.1007/s10098-019-01805-x.
[37] Fido tech. https://fido.tech/.
[38] Bykerk L, Valls Miro J. Vibro-acoustic distributed sensing for large-scale data-driven leak detection on urban distribution mains. Sensors 2022;22(18):6897. https://doi.org/10.3390/s22186897.
[39] Zhang G, Liu M, Shen N, Wang X, Zhang W. The development of the differential MEMS vector hydrophone. Sensors 2017;17(6):1332. https://doi.org/10.3390/s17061332.
[40] Xu J, Chai KT-C, Wu G, Han B, Wai EL-C, Li W, et al. Low-cost, tiny-sized MEMS hydrophone sensor for water pipeline leak detection. IEEE Trans Ind Electron 2018;66(8):6374–82. https://doi.org/10.1109/TIE.2018.2874583.
[41] Yu Y, Safari A, Niu X, Drinkwater B, Horoshenkov KV. Acoustic and ultrasonic techniques for defect detection and condition monitoring in water and sewerage pipes: a review. Appl Acoust 2021;183:108282. https://doi.org/10.1016/j.apacoust.2021.108282.
[42] Leissa AW. Vibration of shells. Scientific and technical information office, vol. 288. National Aeronautics and Space Administration; 1973.
[43] Fahy FJ. Sound and structural vibration: radiation, transmission and response. Elsevier; 2007.
[44] Graf T, Gisler T, Sollberger P, Schälli O. Acoustic wave propagation in water filled buried polyethylene pipes. In: Comsol conference, vol. 7. 2014.
[45] Glentis GO, Angelopoulos K. Leakage detection using leak noise correlation techniques: overview and implementation aspects. In: Proceedings of the 23rd Pan-Hellenic conference on informatics; 2019. p. 50–7.
[46] Gao Y. Leak detection in plastic water pipes. Ph.D. thesis. University of Southampton; 2006.